Int. J. Electrochem. Sci., 8 **(2013)** 5980 - 6004

International Journal of
ELECTROCHEMICAL
SCIENCE
www.electrochemsci.org

Thermodynamics, Quantum and Electrochemical Studies of Corrosion of Iron by Piperazine Compounds in Sulphuric Acid

A. Ousslim[1,2], *A .Chetouani*[1,3,*] , *B. Hammouti*[1], *K. Bekkouch*[2], *S.S. Al-Deyab*[4], *A. Aouniti*[1], *A. Elidrissi*[1].

[1]Laboratory of Applied Chemistry and Environment (LCAE-URAC18), Faculté des Sciences, Université Mohammed Premier, B.P. 717, M-60000 Oujda, Morocco
[2] Laboratoire de Chimie Solide Minérale, Faculté des Sciences, M-60000 Oujda, Morocco
[3] Laboratoire de chimie physique, Centre Régionale des Métiers de l'Education et de Formation "CRMEF", Région de l'Orientale, M-60000 Oujda, Morocco.
4 Petrochemical Research Chair, Chemistry Department, College of Science, King Saud University, P.O. Box 2455, Riyadh 11451, Saudi Arabia
[*]E-mail: ahmedchetouani70@hotmail.com

Received: 23 January 2013 / *Accepted:* 2 March 2013 / *Published:* 1 April 2013

The corrosion inhibition of mild steel in 3.2M H_2SO_4 solution by 1-benzyl piperazine (C2), 1,6-di(1-benzyl piperazine-1-carboxamide)hexane (C4), bis(1-benzyl piperazine) disulfure de thiuram (C5) inhibitors has been studied by potentiodynamic polarization curves and electrochemical impedance spectroscopy (EIS) measurements and weight loss methods. Polarization studies clearly revealed that all the compounds used act as mixed-type inhibitors. The temperature on inhibitory behaviour of C2, C4 and C5 was investigated. Adsorption isotherms were fitted by Langmuir isotherm and adsorption energies (ΔG°_{ads}) and kinetic parameters were evaluated. The correlation between inhibition efficiency and molecular structure of the compounds is investigated by determination of chemical indexes, which were performed using Gaussian03 package software, with density functional theory (DFT) and the correlation functional (B3LYP) in 6-31G* basis.

Keywords: Corrosion; inhibition; piperazine; carbon steel. Sulphuric acid, Quantum chemical, DFT.

1. INTRODUCTION

The corrosion of materials receives more attention either in fundamental academic and industrial concern. The Iron and its alloy have been used widely in a variety of industries. However, it subjects to severe damages by corrosion in aggressive environments, without forgetting, the effects of acid solutions which are generally used for the removal of undesirable products in several industrial

processes [1-4]. As one of the protective measures, corrosion inhibitors are effective to decrease the corrosion rate of metals. The use of inhibitors is one of the most practical methods for protection against corrosion [5-7].

A corrosion inhibitor is a chemical compound which is designed to protect a metal or alloy from corrosion. Usually, organic compounds are widely used in industry for preventing corrosion in acidic environments. Many mechanisms have been proposed for the inhibition of metal corrosion by organic inhibitors [8, 9]. Nowadays, researches in this field focus on the relationship between inhibition efficiency and molecular structures of organic inhibitors, especially the adsorption orientation of the inhibitors on the metal surface [10-13].

The inhibitive power of the organic inhibitors has been interpreted in term of many different characteristics such as molecular size, molecular weight, molecular structure, nature of heteroatom present in the molecule. Various N-heterocyclic compounds with polar groups and/or π-electrons offer good protection of corrosion of steel and iron in acidic media.

The inhibitors molecular can easily adsorb on the metal surface to form a bond between the electron pair and/or the π-electron cloud and the metal thereby reducing the corrosive attack on metals in acidic media.

The processes of adsorption of inhibitors are influenced by the nature and surface charge of the metal, the chemical structure of organic inhibitors, the distribution of charge in the molecule, the type of aggressive electrolyte, type of interaction between organic molecules and the metallic surface and environmental conditions such as temperature and pressure. Physical (electrostatic) adsorption and chemisorptions are the principle type of interaction between organic inhibitor and the metal surface [14-16]

Most of the efficient acid inhibitors are organic compounds that contain mainly sulphur, nitrogen or oxygen atoms in their structure. Generally, it has been assumed that the first stage in the mechanism of the inhibitors action in aggressive acid media is the adsorption of the inhibitors onto the metal surface. Among, these various classes of inhibitors, piperazine compounds exhibit efficient inhibitory effect towards steel in acidic media [17, 18]. To be effective, an inhibitor must be also displace water molecules from the metal's surface and interact with anodic and cathodic reaction sites to retard the oxidation and/or reduction corrosion reaction. So, the inhibition efficiency of organic compounds depends on the concentrations and structure of these inhibitors, the characteristics of the environment in which acts and the mode of interaction with the metal surface [19-22].

In this work, three piperazine derivatives: 1-benzyl piperazine (C2), 1,6-di(1-benzyl piperazine-1-carboxamide)hexane (C4), bis(1-benzyl piperazine) disulfure de thiuram (C5) were tested as corrosion inhibitors of MILD steel in 3.2M H_2SO_4. Weight loss and potentiodynamic polarization were carried out to realise this work. Activation parameters were estimated by studying the effect of temperature in the range 25-60 °C. Correlation is proposed between corrosion inhibition efficiency and a number of quantum molecular properties such as dipole moment (μ), highest occupied (E_{HOMO}) and lowest unoccupied (E_{LUMO}) molecular orbital's and the difference between them (HOMO–LUMO gap) as well as some structural parameters.

2. EXPERIMENTAL

2.1. Materials

The studied compounds 1-benzyl piperazine (C2), 1,6-di(1-benzyl piperazine-1-carboxamide)hexane (C4), bis(1-benzyl piperazine) disulfure de thiuram (C5) were synthesised and analysed by Perkin–Elmer 2400 elemental analyzer. IR spectra samples were run as KBr pellets and 1H NMR spectra on an AC 250 FT spectrometer Bruker. The compounds also were characterized by 1H and by 13C NMR. The molecular structures of the inhibitors are shown in Scheme 1. The choice of such products has been driven by very satisfactory results of their application as inhibitors of iron corrosion.

Synthesis of the compound C4 following operative mode, shows in the schema 1: In a three-necked round-bottomed flask equipped with thermometer, mechanical stirrer, and a reflux condenser, (2.1 g; 2.30 10-2 mol) of 4- benzylpiperazine in 20 mL of THF were placed. The system was kept under nitrogen atmosphere. (1.93 g; 1.15 10-2 mol) of hexamethylene diisocyanate was then added slowly (drop by drop) when the temperature of the system reached 80 °C. To speed up the reaction a single drop of dibutyltin dilaurate (DBTL) was used as catalyst. The temperature was then increased up to 80 °C, and it was kept in this condition for 4 h. The resulted product was precipitated into 50 mL of methanol, filtered and washed with acetone to remove amine formed during the reaction and the diisocyanate that did not react and dried at 60°C to a constant mass. The procedure was performed twice to check the reproducibility. The synthesized product was characterized by spectroscopy techniques and the structure was also confirmed by the elemental analysis

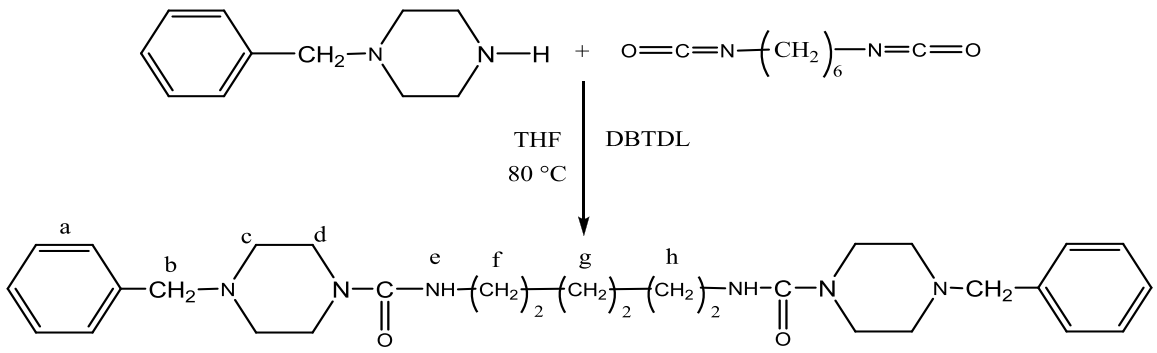

Scheme 1. Reaction synthesis of C4

The compound C5 was synthesised from commercially available C2 according to the following procedure, shows in the schema 2: CS2 (1.8 g; 2.28 9 10-2 mol) was added to a vigorously stirred, cold (<5 °C) solution of 1- benzylpiperazine (2.1 g; 2.30 9 10-2 mol) and triethylamine (2.3 g; 2.30 9 10-2 mol) in ethanol (20 mL) and the stirring and cooling continued for 1 h. To oxidise the dithiocarbamate thus formed to the corresponding thiuram disulfide, I_2 (2.8 g) was then added in portions, complete

discharge of the colour being awaited after each addition. Finally, methanolic I_2 was added drop wise until a yellow colour persisted. The salt, dithiocarbamate, is oxidized to the corresponding thiuram disulfide. The excess of iodine was neutralized with a solution of $Na_2S_2O_3$ (10% by weight). The mixture was then cooled and thiuram disulfide precipitate was filtered and allowed to dry. The solid compound obtained (C5) was yellow in colour, and soluble in organic solvents such as CH_2Cl_2 and $CHCl_3$. Yield: 3.70 g (80%); m.p = 136 _C. 1H-NMR in $CDCl_3$ (d ppm). 7.3 (10Ha); 4.27 (4Hb); 3.54 (4Hc), 2.59 (4Hd); the Hc and Hd are coupled. IR: max/cm-1 1280–1190 (NCSS). The chemical structures of the inhibitors are shown in Scheme 1.

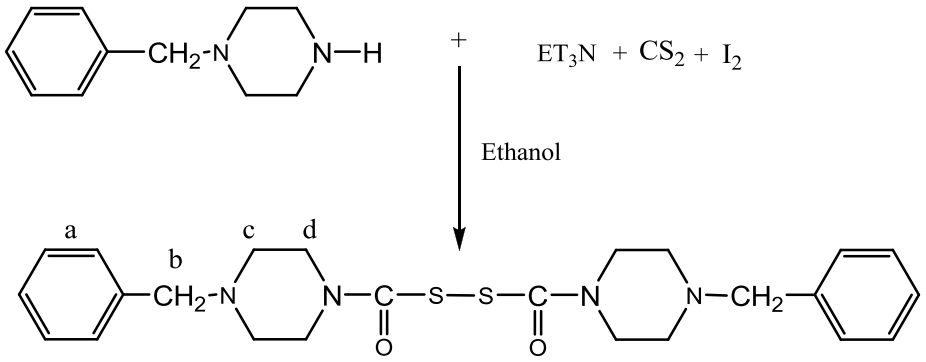

Scheme 2. Reaction synthesis of C5

The molecular inhibitors C2, C4 and C5 were minimised by MM2 method. The MM2 force field method is available of ChemBio3D. MM2 is most commonly used for calculating properties of organic molecular models. The MM2 procedures described assume that you understand how the potential energy surface relates to conformations of your model. In ChemBio3D 12.0, the MM2 atom type is used for force field calculations and used only in building models were shows in schema 3. Table 2 brings together the different parameters to calculate from the MM2 method, such as. Stretch, Bend, Stretch-Bend, Torsion, Non-1,4 VDW, 1,4 VDW Dipole/Dipole and Total Energy.

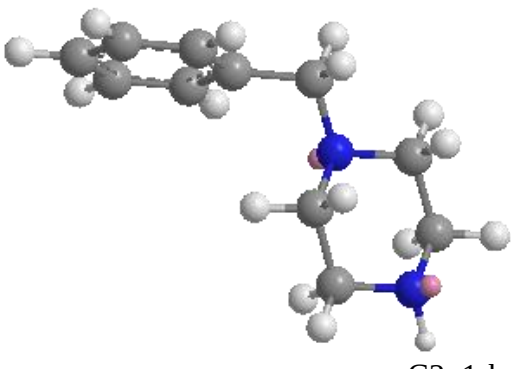

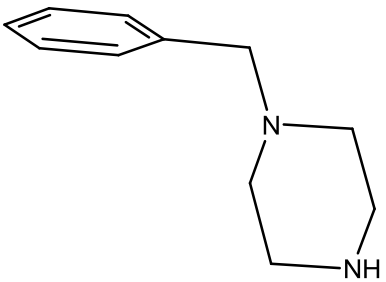

C2: 1-benzyl piperazine

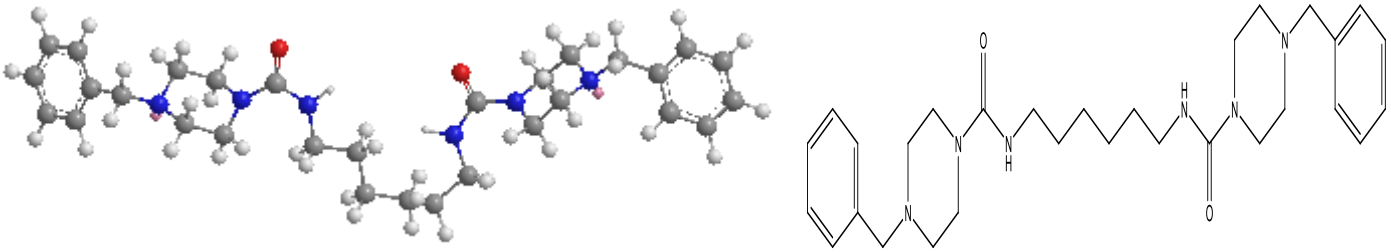

C4 : 1,6-di(1-benzyl piperazine -1-carboxamide)hexane

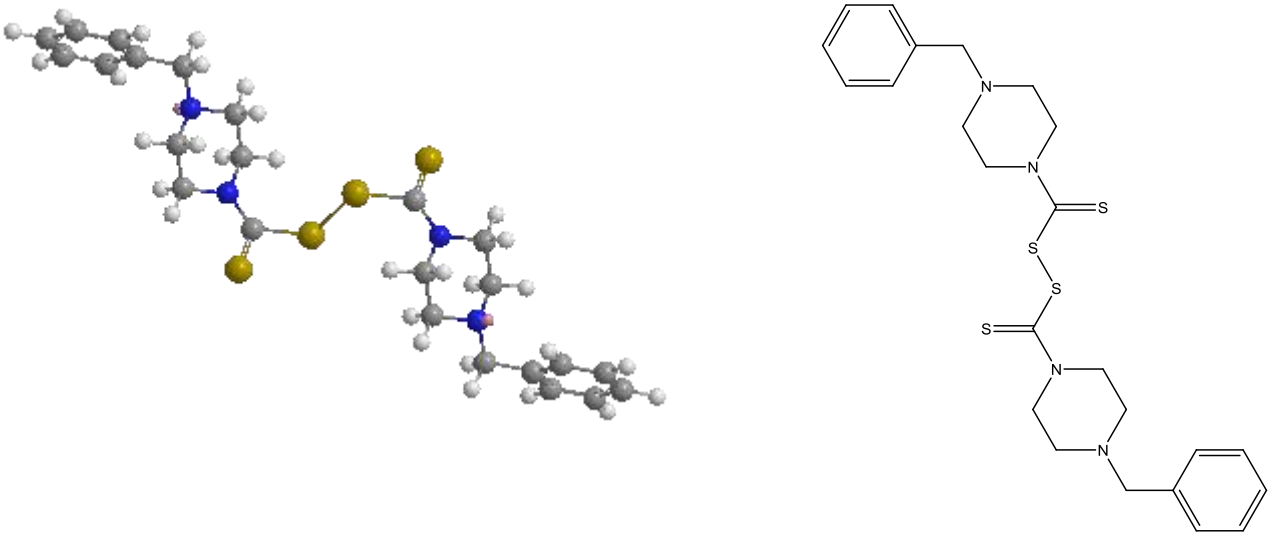

C5 : bis(1-benzyl piperazine) disulfure de thiuram

Scheme 3. Molecular structure of different inhibitors

Table 1. Parameters Minimize Energy Computation of C2, C4 and C5

	C2	C4	C5
Stretch	0.7886	1.9709	1.9890
Bend	1.1979	13.0388	8.4754
Stretch-Bend	0.1962	0.6626	0.5378
Torsion	-7.1688	6.3138	-12.4974
Non-1,4 VDW	2.4593	-7.3675	-3.9735
1,4 VDW	10.2664	24.0064	22.6006
Dipole/Dipole	0.0103	-11.1990	-4.3429
Total Energy (kcal/mol)	2.8106	27.4260	12.7890

The experiments were performed with mild steel with the following composition table 2. Samples were polished with emery paper up to 1200 grade, and then washed with double-distilled water, and degreased with ethanol.

The acid solutions (3.2M H_2SO_4) were prepared by dilution of a Merck analytical reagent grade 98 % H_2SO_4 and density 1.84g/cm^3 (20°C) with double-distilled water. The concentration range of inhibitor was 10^{-5} M to 10^{-3} M.

Table 2. Chemical composition of mild steel.

Elements	Fe	C	Si	P	Mn	S	Al
% en masse	99.21	0.21	0.38	0.09	0.05	0.05	0.01

2.2. Corrosion tests

For the weight loss measurements, the experiments were carried out in solution of 3.2 M H_2SO_4 (uninhibited and inhibited) on mild steel. Sheets with dimensions 2.5 x 2cm x 0.5cm were used. They were polished successively with different grades of emery paper up 1200 grade. Each run was carried out in a glass vessel containing 100 ml test solution. A clean weight mild steel sample was completely immersed at an inclined position in the vessel. After 4 h of immersion in 3.2 M H_2SO_4 with and without addition of inhibitor at different concentrations, the specimen was withdrawn, rinsed with distilled water, washed with ethanol, dried and weighted. The weight loss was used to calculate the corrosion rate in milligrams per square centimetre per hour. All experiments were carried out in freshly prepared solution at constant temperatures, 25, 30, 40, 50°C and 60 ± 0.1 °C using a thermostat.

For electrochemical measurements, a conventional three-electrode glass cell with a platinum counter electrode and a saturated calomel electrode (SCE) as reference was used. Mild steel cylindrical rod of the same composition as working electrode was pressure fitted into a polytetrafluoroethylene holder (PTFE) to avoid any infiltration of electrolyte then exposing only 1 cm^2 surface to the aggressive solution. The test solution was thermostatically controlled at 25 °C in air atmosphere without bubbling. All potentials were measured against SCE.

Potentiodynamic polarisation experiments were conducted using an EGG Potentiostat–Galvanostat (model 263A), coupled to a computer equipped with the software 352 Soft Corr^{TM} III. The potentiodynamic current–potential curves were recorded by changing the electrode potential automatically from -800 to -100 mV at a scanning rate of 1 mVs^{-1}. Before measurement, the working electrode was immersed in the test solution at the natural potential (open circuit potential) for 30 min, in which time a steady state was reached. The WE was polarized at -800 mV for 10 min in order to remove oxide film from the electrode. The linear Tafel segments of the anodic and cathodic curves were extrapolated to the corrosion potential to obtain the corrosion current densities (i_{corr}). De-oxygenation of the test solution with pure nitrogen was carried out prior to starting the polarization measurements. Each test was run in duplicate to verify the reproducibility and the average values are reported.

The data in Tafel region have been processed for evaluation corrosion kinetic parameters by plotting the polarization curves. The linear Tafel segments, in a large domain of potential, of the

cathodic curves were extrapolated to the corresponding corrosion potentials to obtain the corrosion current values. The inhibition efficiency was evaluated using the relationship (1):

$$IE_{I-E} = \frac{i_{corr}^{0} - i_{corr}}{i_{corr}^{0}} \times 100 \quad (1)$$

i_{corr}^{0} and i_{corr} are the corrosion current densities values without and with inhibitors, respectively.

The values of the degree of surface coverage (θ) have been obtained from polarization curves for various concentrations of inhibitors. Here, θ can be given as (2) [15]:

$$\theta = 1 - \frac{i_{corr}}{i_{corr}^{0}} \quad (2)$$

The electrochemical impedance spectroscopy measurements were carried out using a transfer function analyzer (Voltalab PGZ 100), with a small amplitude ac. signal (10 mV/ms), over a frequency domain from 100 kHz to 10 mHz at 25 °C on air atmosphere with 5 points per decade. Computer programs automatically controlled the measurements performed at rest potentials after 1 h of immersion at E_{corr}. The impedance diagrams were given in the Nyquist representation. To determine the impedance parameters of the mild steel specimens in acidic solution, the measured impedance data were analyzed using Bouckamp program based upon an electric equivalent circuit [16]. The inhibition efficiency of the inhibitors has been determined from the relationship (3):

$$IE_{imp}\% = \frac{R_t - R_t^{0}}{R_t} \times 100 \quad (3)$$

R_t^{0} and R_t are the charge transfer resistance values in the absence and in the presence of inhibitors, respectively.

2.3. Computational method

The density functional theory (DFT) is presently the most successfull (and also the most promising) approach to compute the electronic structure of matter. Its applicability ranges from atoms, molecules and solids to nuclei and quantum and classical fluids. In its original formulation, the density functional theory provides the ground state properties of a system, and the electron density plays a key role. DFT predicts a great variety of molecular properties: molecular structures, vibrational frequencies, atomization energies, ionization energies, electric and magnetic properties, reaction paths, etc. The original density functional theory has been generalized to deal with many different situations: spin polarized systems, multi-component systems such as nuclei and electron hole droplets, free energy at finite temperatures, superconductors with electronic pairing mechanisms, relativistic electrons, time-dependent phenomena and excited states, bosons, molecular dynamics, etc.

All theoretical calculations were performed using, Gaussian 3 package software's, DFT (density functional theory) with the Beck's three parameter exchange functional along with the Lee–Yang–Parr nonlocal correlation functional (B3LYP) [20–22] with 6- 31G* basis set is implemented in Gaussian 03 program package [23]. This approach is shown to yield favourable geometries for a wide variety of systems. This basis set gives good geometry optimizations. The geometry structure of piperidine derivatives was optimized under no constraint. The following quantum chemical parameters were calculated from the obtained optimized molecular structure: the energy of the highest occupied molecular orbital (E_{HOMO}), the energy of the lowest unoccupied molecular orbital (E_{LUMO}), the energy band gap ($\Delta E_{gap} = E_{HOMO} - E_{LUMO}$), the dipole moment ($\mu$) and the total energy ($E_T$).

3. RESULTS AND DISCUSSION

3.1. Effect of immersion time

In this study, we were interested in the rate of inhibition of inhibitors during time intervals between 30 min and 6 h. Table. 3. represents the variation of weight loss and E% with time of mild steel immersed in 3.2 M H_2SO_4 in the absence and presence of (C4) and (C5) at 10^{-3}M. The data in table 3. shows that the weight loss (mg/cm^2) increases with time along a period of 6 hours (immersion time) both in acid and inhibited acid. The corrosion rate in an acid medium, in the absence of inhibitor is relatively stable after four hours of immersion. From the weight loss results, the corrosion rate (CR), the inhibition efficiency ($\eta_{WL}(\%)$) of the inhibitor and degree of surface coverage (θ) were calculated using equations 4, 5 and 6;

$$C_R = \frac{W_b - W_a}{At} \quad (4)$$

$$\eta_{WL}(\%) = \left(1 - \frac{w_i}{w_0}\right) \times 100 \quad (5)$$

$$\theta = 1 - \frac{w_i}{w_0} \quad (6)$$

where W_b and W_a are the specimen weight before and after immersion in the tested solution, w_0 and w_i are the values of corrosion weight losses of carbon steel in uninhibited and inhibited solutions, respectively, A the total area of the carbon steel specimen (cm^2) and t is the exposure time (h) and θ is the degree of surface coverage of the inhibitor.

Table 3. Effect of time of mild steel and E% in 3.2M H_2SO_4 with and without inhibitors

T (h)	H_2SO_4 $10^{-4}\times CR$ (mg cm^{-2} h^{-1})	η_{WL} (%)	C4 $10^{-4}\times CR$ (mg cm^{-2} h^{-1})	η_{WL}(%)	C5 $10^{-4}\times CR$ (mg cm^{-2} h^{-1})	η_{WL} (%)
0,5	2,7	-	1.1	59	0.9	66
1	3.5	-	0.5	86	0.7	80
2	3.7	-	0.2	94	0.4	89
3	4.0	-	0.1	97	0.3	92
4	4.4	-	0.09	98	0.2	95
5	4.4	-	0.06	98	0.1	98
6	4.4	-	0.04	99	0.1	98

In the presence of inhibitors, the corrosion rate is almost constant from the first hour of immersion in aggressive solution. Furthermore, the inhibition efficiency of the tested compounds believed for the first one hour of immersion and after it stabilised on its maximum value. Finally, we can conclude that the net decrease of weight loss in the presence of 1-benzyl piperazine (C2), 1,6-di(1-benzyl piperazine-1-carboxamide)hexane (C4), bis(1-benzyl piperazine) disulfure de thiuram (C5) is a importance indicator that these compounds play the role of efficient inhibitors of mild steel in test solutions.

3.2 Effect of inhibitor concentration.

Weight loss of C-steel, in mg.cm^{-2} of the surface area, was determined at different concentration in the absence and presence of 1-benzyl piperazine (C2), 1,6-di(1-benzyl piperazine-1-carboxamide)hexane (C4), bis(1-benzyl piperazine) disulfure de thiuram (C5) in 3.2M H_2SO_4 after 4 h at 298 K.

The values of η_{WL}(%) for two inhibitors are given in Table 4. This show that the inhibition efficiency increases with the increasing inhibitor concentration. These results reveal that the compounds under investigation are fairly efficient inhibitors for C-steel dissolution in 3.2M H_2SO_4 solution.

The results show that corrosion rates decrease with increase of (C2), (C4), and (C5). In the presence of C2, C4 and C5 at 10^{-3}M, the corrosion rate is observed to reduce significantly and we can conclude that the compounds have the best inhibitory efficiencies in the three corrosive environments. The inhibition efficiency is found to increase with increasing concentration of C2, C4 and C5 up to 10^{-3}M to attain 88%, 98% and 95%, respectively.

The inhibition of corrosion of C-steel by C2, C4 and C5 can be explained in terms of adsorption on the metal surface. These compounds can be adsorbed by the interaction between lone pairs of electrons of nitrogen atoms of the inhibitors and the metal surface. This process is facilitated by the presence of vacant orbital of low energy in iron atom, as observed in the transition group

elements. Careful inspection of these results showed that, the ranking of the inhibitors according to $\eta_{WL}(\%)$ is as follows: C4 > C5> C2 for the same concentration.

Table 4. Gravimetric results of steel in acid solutions 3.2M H_2SO_4 at different concentration of C2, C4 and C5 (298 K & 4 h)

Inhibitors	Conc (M)	$10^{-4}\times CR$ (mg cm^{-2} h^{-1})	$\eta_{WL}(\%)$	θ
Blank	1	4.4	-	-
C2	10^{-5}	2.5	43	0.43
	510^{-5}	2.1	52	0.52
	10^{-4}	1.3	70	0.70
	510^{-4}	0.9	79	0.79
	10^{-3}	0.5	88	0.88
C4	10^{-5}	0.9	79	0.79
	510^{-5}	0.6	86	0.86
	10^{-4}	0.4	91	0.91
	510^{-4}	0.3	93	0.93
	10^{-3}	0.09	98	0.98
C5	10^{-5}	0.5	88	0.88
	510^{-5}	0.4	91	0.91
	10^{-4}	0.3	93	0.93
	510^{-4}	0.3	93	0.93
	10^{-3}	0.2	95	0.95

3.3. Effect of temperature.

The effect of temperature on the inhibited acid–metal reaction is highly complex because many changes occur on the metal surface, such as rapid etching and desorption of the inhibitor and the inhibitor itself, in some cases, may undergo decomposition and/or rearrangement. However, it provides the ability of calculating many thermodynamic functions for the inhibition and/or the adsorption processes which contribute in determining the type of adsorption of the studied inhibitors[23] .

Temperature can affect the mild steel corrosion in the acidic media in the presence and absence of inhibitor. Generally the corrosion rate increases with the rise of the temperature. To determine the action energy of the corrosion process, In order to gain more information about the type of adsorption and the effectiveness of the studied inhibitors at higher temperatures, gravimetric experiments were performed at different temperatures (293–333 °K) for the steel electrode in 3.2M H_2SO_4 without and with selected concentrations at 10^{-3}M of 1,6-di(1-benzyl piperazine-1-carboxamide) hexane (C4), bis(1-benzyl piperazine) disulfure de thiuram (C5) for a 4 h reaction period. The corresponding results are given in Table 5. The activation energies for the corrosion process were calculated from the Arrhenius equation (7):

$$W = A \exp\left(-\frac{E_a}{RT}\right) \quad (7)$$

where E_a represents the apparent activation energy, R the gas constant, T the absolute temperature, A the pre-exponential factor and W the corrosion rate, obtained from the weight loss method.

Table 5. Inhibition efficiency obtained from the corrosion rate at 10^{-3}M of different inhibitors in 3.2M H_2SO_4 at different temperature at 4h immersion period.

T (°C)	H_2SO_4		C4		C5	
	W ($mg.cm^{-2}.h^{-1}$)	E (%)	W ($mg.cm^{-2}.h^{-1}$)	E (%)	W ($mg.cm^{-2}.h^{-1}$)	E (%)
25	4,4	-	0,09	98	0,2	95
30	7,1	-	0,5	93	0,7	90
35	10,6	-	1,0	90	1,2	89
40	14,9	-	2,3	84	3,2	78
45	22,4	-	4,8	78	8,9	60
50	30,4	-	12,2	60	16,6	45
60	56,5	-	29,4	48	37,7	33

In the absence and presence of different inhibitors, the corrosion rate of mild steel increases with rise in temperature and the inhibition efficiency decreases to reach a value of 48% and 33% at 333 K for C4 and C5 at 4h immersion period. It is clear also, that the increase of corrosion rate is more pronounced with the rise of temperature for the blank solution. In the presence of the tested molecules, W_{corr} is reduced even at high temperature. E (%) passed from 98 to 48% and 95 to 33% for C4 and C5 respectively, when temperature rises from 298 to 333 K at 10^{-3} M.

We note that the efficiency of the inhibitors tested depends on the temperature and decreases with the rise of temperature from 298 to 333 K

Arrhenius plots for the corrosion rate of mild steel are given in Figure. 1. Values of E_a for mild steel in 3.2M H_2SO_4 in the absence and presence of various concentrations of 1,6-di(1-benzyl piperazine-1-carboxamide)hexane (C4), bis(1-benzyl piperazine) disulfure de thiuram (C5) were determined from the slopes of ln W versus 1000/T plots.

Enthalpy (ΔH_a^0) and entropy (ΔS_a^0) activation energies may be evaluated by the alternative formulation (eq. 8), where W refers to the corrosion rate, R the gas constant, T the absolute temperature, A the pre-exponential factor, h is Plank's constant and N is Avogadro's number.

$$W = \frac{RT}{Nh} \exp\left(\frac{\Delta S_a^o}{R}\right) \exp\left(-\frac{\Delta H_a^o}{RT}\right) \quad (8)$$

The plots of ln(W/T) versus 1/T shown in figure 5 . Straight lines are obtained with a slope of ($-\Delta H_a^0/R$) and an intercept of (Ln (R/Nh) + $\Delta S_a^0/R$). The calculated values of E_a, ΔH_a^0 and ΔS_a^0 are collected in Table 6.

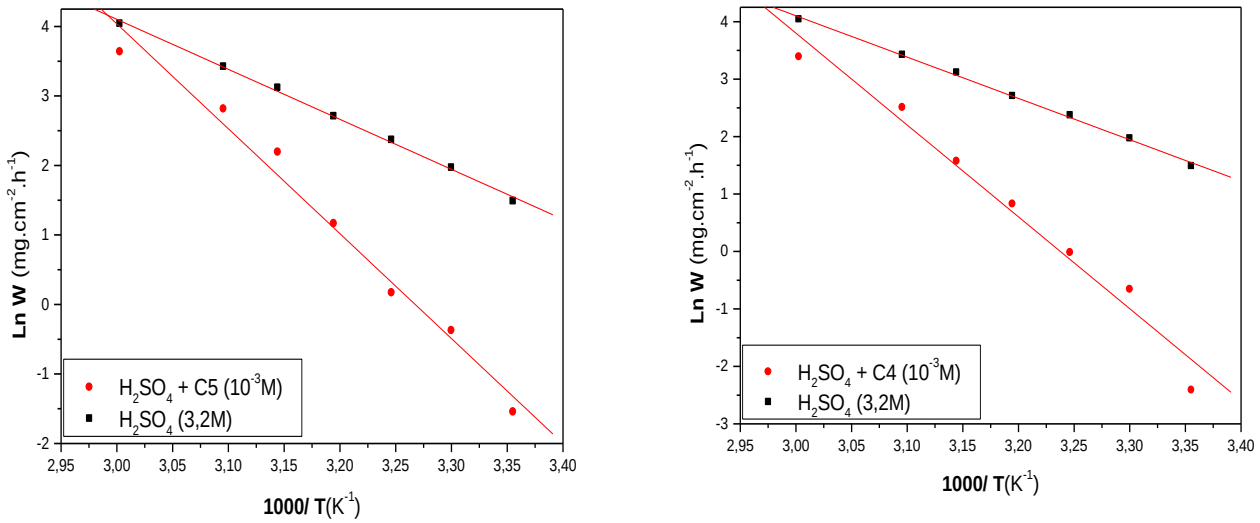

Figure 1. Arrhenius plots of steel for 10^{-3}M of C4 and C5 in 3.2M H_2SO_4.

The value of apparent activation energy E_a of hydrogen evolution reaction for 3.2M H_2SO_4 without an inhibitor (59.75 kJ.mol^{-1}). In the presence of C4 and C5 inhibitors, the process of metal dissolution is characterized by an activation energy less than that in the uninhibited 3.2M H_2SO_4 (Table 6). The addition of inhibitor modified the values of E_a; this modification may be attributed to the change in the mechanism of the corrosion process in the presence of adsorbed inhibitor molecules [7, 12, 21, 24-26].

The addition of these compounds to the corrosive solution is accompanied by an increase in activation energy; this could be attributed to the presence of an energy barrier for the corrosion reaction due to the existence of inhibitor to interphase metal / electrolyte, which shows a change in the mechanism of transition metal in solution. The lower value of the activation energy of the process in an inhibitor's presence when compared to that in its absence is attributed to its chemisorptions, while the opposite is the case with physical adsorption [27, 28].

The lower value of the E_a was attributed to a slow rate of inhibitor adsorption with a resultant closer approach to equilibrium during the experiments at the higher temperature. But, w can explained that the decrease in activation energy of corrosion at higher levels of inhibition arises from a shift of the net corrosion reaction from that on the uncovered part on the metal surface to the covered one [28, 29]. we found also that organic molecules inhibit both the anodic and cathodic partial reactions on the electrode surface and a parallel reaction takes place on the covered area, but that the reaction rate on the covered area is substantially less than on the uncovered area [30, 31].

A straight lines are obtained with a slope of ($-\Delta H_a^0/R$) and an intercept of (Ln $R/Nh + \Delta S_a^0/R$) from which the values of ΔH_a^0 and ΔS_a^0 are calculated, are listed in Table 6. The relationship between the activation energy E_a and activation heat ΔH_a^0 against the concentration of inhibitors C4 and C5 is shown in Fig. 2. From the data obtained in Table 6, it seems that E_a and ΔH_a^0 vary in the same manner, these results agree those obtained in the literature [5, 32, 33] this result allows verification of the known thermodynamic reaction between the E_a and ΔH_a^0 (Eq.9).:

$$\Delta H_a^\circ = E_a - RT \quad (9)$$

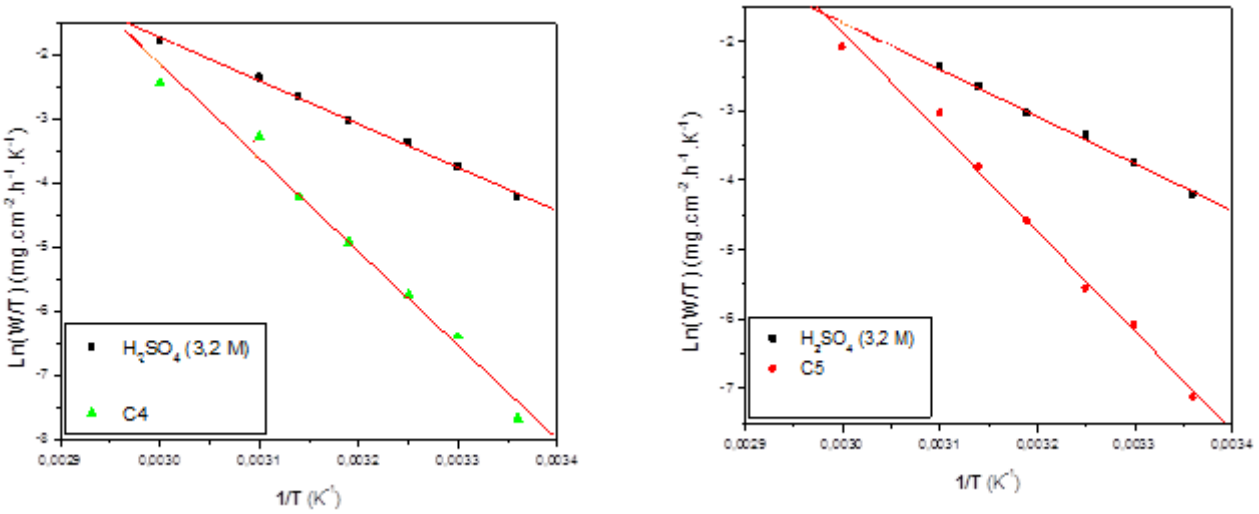

Figure 2. The variation of Ln (W / T) ~ f (1 / T) of the steel in H_2SO_4 with and without C4 and C5

Table 6. Activation parameters for steel in 3.2M H_2SO_4 in the absence and presence of C4 and C5

	Linear regression Coefficient α	E_a (kJ/mol)	$\Delta H°_a$ (kJ/mol)	$\Delta S°_a$ (J/mol.K)
Blank	0,998	59,75	57,20	-40,25
C4	0,991	125,56	122,9	156,4
C5	0,984	137,15	134,5	188,2

The positive signs of the enthalpies (ΔH_a^0) reflect the endothermic nature of the steel dissolution process (Table 5). Large and negative values of entropies (ΔS_a^0) imply that the activated complex in the rate determining step represents an association rather than a dissociation step, meaning that a decrease in disordering takes place on going from reactants to the activated complex and suggesting that the dissolution reaction will be more blocked sites from the metal surface. The increase in entropy (ΔS_a^0) in the presence of an inhibitor implies. This result indicates that the corrosion. changes from a more ordered system. a disordered system [34, 35].

3.4. Potentiodynamic study

Several methods may be used in polarization of specimens for corrosion testing. Potentiodynamic polarization is a technique where the potential of the electrode is varied at a selected rate by application of a current through the electrolyte. It is probably the most commonly used polarization testing method for measuring corrosion resistance and is used for a wide variety of functions [31, 36].

Polarization measurements have been carried out in order to gain knowledge concerning the kinetics of the anodic and cathodic reactions. Potentiodynamic curves are obtained in the presence and absence of the studied inhibitors, after pre-polarizing the electrode at its E_{corr} for one hour, thereafter pre-polarized at -800 mV for 10 min. After this scan, the potential was swept stepwise from the most cathodic potential to the anodic direction. Fig. 3 shows polarization curves for C38 steel in 3.2M H_2SO_4 without and with different concentrations of 1,6-di(1-benzyl piperazine-1-carboxamide)hexane (C4), bis(1-benzyl piperazine) disulfure de thiuram (C5). The anodic and cathodic current–potential curves were extrapolated up to their interaction point where corrosion current density (I) and corrosion potential (E) are obtained.

The electrochemical parameters such as corrosion current density (I), corrosion potential (E), cathodic Tafel slopes (β_c) and inhibition efficiency obtained from polarization measurements are listed in Table 7.

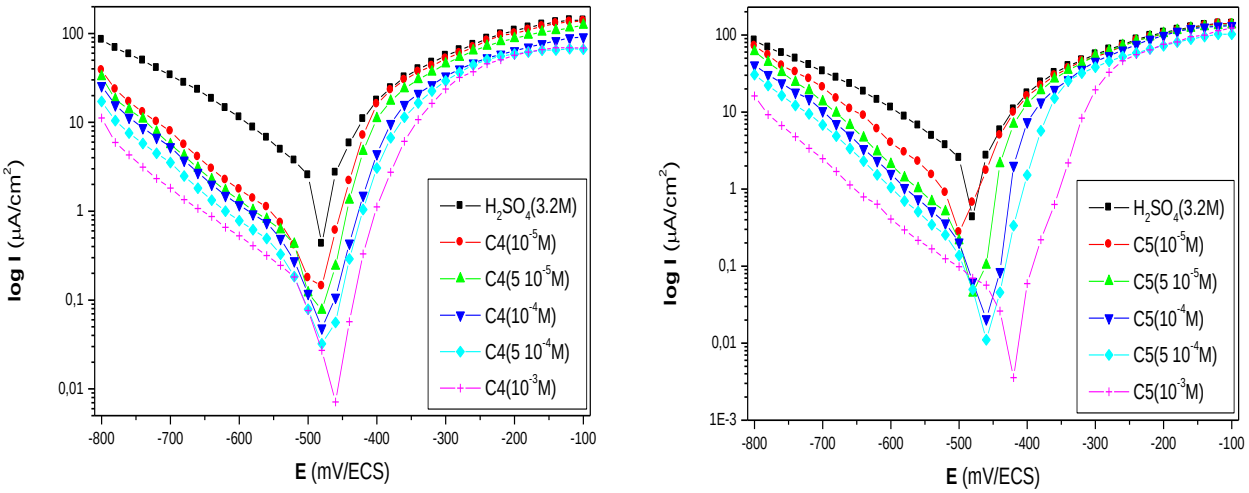

Figure 3. Polarisation curves of steel in 3.2M H_2SO_4 at different concentrations of C3, C4 and C5 at 298 K

Examination of curves indicate In general, the presence of increasing amount of C4 and C5 to decrease in both the cathodic and anodic current densities, but with more pronounced decrease in the cathodic domain at elevated concentrations. In contrast, E_{corr} trends towards more anodic direction in the case of C4 and C5 with a both decrease in the anodic and cathodic branches. The values I_{corr} of steel in the inhibited solution are smaller than those for the inhibitor free solution (Table 7). The

parallel cathodic Tafel plots obtained in Fig. 3 indicate that the hydrogen evolution is activation-controlled and the reduction mechanism is not affected by the presence of inhibitor. The change in cathodic Tafel slope (β_c) values (Table 2), suggest that the reaction mechanism of the hydrogen reduction is not the same in the absence and presence of inhibitor.

These inhibitors seem to be mixed-type inhibitor with marked cathodic behaviour. Cathodic Tafel slopes b_c, were approximately constant, meaning that the inhibiting action of these molecules occurred by simple blocking of the available surface area; i.e. the inhibitors decreased the surface area for hydrogen evolution without affecting the reaction mechanism

Table 7. Potentiodynamic polarisation parameters of the mild steel in 3.2M H_2SO_4 without and with C4 and C5 at various concentrations at 298 K.

Inhibitors	C (M)	E_{corr} (mV/ECS)	b_C (mV/dec)	I_{corr} ($\mu A/cm^2$)	E (%)
Blank	3.2	-474	210	1948	-
C4	10^{-5}	-471	132	330	83
	510^{-5}	-471	138	208	89
	10^{-4}	-464	146	166	91
	510^{-4}	-453	158	109	94
	10^{-3}	-446	181	67	96
C5	10^{-5}	-496	152	637	67
	510^{-5}	-494	147	324	83
	10^{-4}	-477	138	147	92
	510^{-4}	-441	136	68	96
	10^{-3}	-406	132	23	99

From electrochemical polarisation measurements: It is clear from the results that the addition of inhibitor causes a decrease of the current density. The lower value of i_{corr} is obtained at 10^{-3} M; so the inhibition efficiency reaches the maximum of 96% and 99 % for C4 and C5, respectively. The results obtained by this electrochemical method are almost similar to those obtained by the gravimetric method.

3.5. Electrochemical impedance spectroscopy (EIS)

Potentiodynamic electrochemical impedance spectroscopy is the technique for characterisation of electrochemical responses of interfacial processes and structures. EIS acquires variable frequency responses in alternating current and a potentiodynamic dc voltammogram in the same potential scan, by probing the electrochemical interface with streams of mutually coordinated wavelets. The potentiodynamic impedance spectrum by a Voltalab connected to a computer. The object is placed in a common three-electrode electrochemical cell and the spectra are usually recorded, which give additional information on the extent of reversibility of different constituent processes that contribute to the frequency response of a nonstationary electrochemical interface. Impedance measurements provide

information on both the resistive and capacitive behaviour of the interface and makes possible to evaluate the performance of the studied inhibitors. Before each EIS experiments, as done with Tafel experiments, the electrode was allowed to corrode freely for an hour to obtain a steady-state open circuit potential, corresponding to the corrosion potential, E_{corr}, of the working electrode. From the various impedance data, interfaces are often described by equivalent circuits involving resistors, capacitors and sometimes inductances. The various electrochemical reactions involve the formation of electrical double layer. The inhibitive performances of organic inhibitors are widely discussed on the basis of EIS characteristics [19, 20, 26]. EIS technique has been used to evaluate the efficiency of some organic substances as inhibitors for corrosion of iron in acids and others [19, 20, 25, 26, 37, 38].

Impedance measurements of the mild steel electrode at its open circuit potential after 1 h of immersion in 3.2M H_2SO_4 solution with and without 1,6-di(1-benzyl piperazine-1-carboxamide)hexane (C4), bis(1-benzyl piperazine) disulfure de thiuram (C5) inhibitors were performed over the frequency range from 10 kHz to 40 mHz.

the deduced impedance parameters as transfer-resistance Rt ($\Omega.cm^2$), frequency f_m (Hz), double layer capacitance C_{dl} (F/cm^2) and corresponding inhibition efficiency (E_{Rt}%) are gathered in table.6. It is seen from this figure (7), the impedance diagrams does show semi-circles. We remark that the increase of Rt and decrease of double-layer capacitance (C_{dl}) and the efficiency increases when the concentration 1,6-di(1-benzyl piperazine-1-carboxamide)hexane (C4), bis(1-benzyl piperazine) disulfure de thiuram (C5) increases.

Table 8. Characteristic parameters evaluated from EIS diagrams with and without *C4 and C5* at different concentrations.

Inhibitor	C (M)	Rs (Ω.cm2)	Rt (Ω.cm2)	f_{max} (Hz)	Cdl (µF/cm2)	E_Z (%)
blank	3.2	1.0	4.3	400.2	92.6	-
C4	10^{-5}	0.9	16.8	140.2	67.4	74
	5.10^{-5}	1.0	22.6	128.5	54.9	81
	10^{-4}	1.1	34.2	97.89	47.6	87
	5.10^{-4}	1.0	46.2	88.56	38.9	90
	10^{-3}	1.1	64.3	80.77	30.6	93
C5	10^{-5}	0.9	27.2	88.44	66.1	84
	5.10^{-5}	0.9	38.1	77.38	54.0	89
	10^{-4}	1.1	43.8	73.88	49.1	90
	5.10^{-4}	1.0	50.1	73.85	43.0	91
	10^{-3}	1.0	78.8	71.22	28.3	94

The charge-transfer resistance (R_t) values are calculated from the difference in impedance at lower and higher frequencies. The charge transfer-resistances (Rt) values were calculated from the difference in impedance at low and high frequencies [20, 25, 26, 37, 38]. The double layer capacitance (C_{dl}) was obtained at the frequency f_m at which the imaginary component of the impedance is maximal ($Z_{i,\,max}$) by the equation (10):

$$C_{dl} = \frac{1}{2\pi f_m . R_t} \quad (10)$$

Inspections of these values reveal that each impedance diagram consists of a large capacitive loop at high frequency (HF) with one capacitive time constant. As usually indicated in the EIS study, the HF capacitive loop is related to the charge transfer process of the metal corrosion and the double-layer behaviour. The value of C_{dl} decreases in the presence of C4 and C5, suggesting that the inhibitors molecules function by adsorption at the metal solution/interface. The decrease in C_{dl} may be due also to the adsorption of this compound on the metal surface leading to the formation of film from acidic solution [22, 31, 39]. The values of inhibition's efficiency increase with inhibitor concentration at a maximum value 93% and 94% for C4 and C5 respectively at 10^{-3}M.In fact, the presence of 1,6-di(1-benzyl piperazine-1-carboxamide)hexane (C4), bis(1-benzyl piperazine) disulfure de thiuram (C5) compounds enhances the value of R_t in acidic solution. Values of double layer capacitance are also brought down to the maximum extent in the presence of C 4 and C5 and the decrease in the values of C_{dl} follow the order similar to that obtained for I_{corr} in this study. We note a agreement between the values of inhibition efficiency determined gravimetrically and by electrochemical impedance spectroscopy.

3.6. Adsorption isotherm

Successful representation of the dynamic adsorptive separation of solute from solution onto an adsorbent is dependent upon a good description of the equilibrium separation between the two phases. An equilibrium is established when the amount of solute being adsorbed onto the adsorbent is equal to the amount being desorbed. The equilibrium solution concentration remains constant. Plotting solid-phase concentration against liquid-phase concentration graphically depicts the equilibrium adsorption isotherm. Several theories of adsorption equilibrium, used to describe these isotherms, are available in the literature.

The adsorption isotherm can be determined if the inhibitor effect is due mainly to the adsorption on metallic surface (i.e. to its blocking). The adsorption isotherm type can provide additional information about the tested compounds properties. The fractional coverage surface (θ) can be easily determined from gravimetric results shown in Table 4. The adsorption isotherms models considered were as described in reference [40] (Eq.11,12,13 and 14).:

Temkin isotherm $$exp\,(f.\theta) = K_{ads}\, C_{inh} \quad (11)$$

Langmuir isotherm $$\frac{\theta}{1-\theta} = K_{ads} C_{inh} \quad (12)$$

Frumkin isotherm $$\frac{\theta}{1-\theta}\exp(-2f\theta) = K_{ads} C_{inh} \quad (13)$$

Freundlich isotherm $\theta = K_{ads}\, C_{inh}$ (14)

Where K_{ads} is the equilibrium constant of the adsorption process, C_{inh} is the inhibitor concentration and f is the factor of energetic inhomogeneity. The linear coefficient regression, r was used to choose the isotherm that best fit experimental data (Table 3).

The best fitted straight line (strong correlation with r>0.999) is obtained for the plot of C_{inh}/θ vs. C_{inh} with slopes around unity. This suggests that the adsorption of the studied inhibitors on metallic surface obeyed to the Langmuir's adsorption isotherm model (Fig. 4). The Langmuir isotherm theory assumes monolayer coverage of adsorbate over a homogenous adsorbent surface. Graphically, a plateau characterizes the Langmuir isotherm. Therefore, at equilibrium, a saturation point is reached where no further adsorption can occur. A basic assumption is that sorption takes place at specific homogeneous sites within the adsorbent. Once a dye molecule occupies a site, no further adsorption can take place at that site [5, 41] .

The best correlation coefficient (R^2) value is obtained by Langmuir adsorption isotherm. The surface coverage θ is related to the equilibrium adsorption constant k_{ads} and the concentration of inhibitor C by the rearranged Langmuir equation. While the Langmuir isotherm supposed monolayer physical adsorption of the formed complex, the equation leads to ΔH_{ads}, where A is a temperature independent constant, C the inhibitor concentration and ΔH_{ads} is the adsorption heat. (Eq.5).

$$\frac{\theta}{1-\theta} = AC\exp(-\frac{\Delta H_{ads}}{RT}) \quad (15)$$

From the intercepts of the straight lines C_{inh}/θ vs. C_{inh}, K_{ads} value can be calculated. The constant of adsorption, K_{ads}, is related to the standard free energy of adsorption, $\Delta_{ads}G^0$, by the following equation (16), where 55.55 represent the concentration of water in solution in mol L^{-1}, R is the universal gas constant and T is the absolute temperature

$$K_{ads} = \frac{1}{55{,}55}\exp(-\frac{\Delta_{ads}G^{\circ}}{RT}) \quad (16)$$

The standard free energy of adsorption, $\Delta_{ads}G^0$ can be calculated. We remark that the best fit was obtained with the Langmuir isotherm (Figure. 4), the slope is too close unity (1.018) with R^2= 0.9999.

The negative values of $\Delta_{ads}G^0$ ensure the spontaneity of the adsorption process and stability of the adsorbed layer on mild steel surface. It is well known that values of $\Delta_{ads}G^0$ of order of 20 kJ mol^{-1} or lower are consistent with the electrostatic interaction between the charged molecules and the charged metal and indicate a physisorption; while those of order of 40 kJ mol^{-1} involve charge sharing or transfer from the inhibitor molecules to the metal surface to form a coordinate bond (chemisorptions). The higher values are associated with chemisorptions.

Values of $\Delta_{ads}G^0$, as reported in Table 4, are -38.78 and -40.85 for *C4* and *C5*, respectively. It is suggested that the adsorption mechanism of the investigated inhibitors on the mild steel surface in 3.2

M H_2SO_4 solution involves two types of interaction; chemisorptions and physisorption. The mechanism of inhibitors action is their adsorption onto the metal surface to block the interface reactivity and then retard or stop the corrosion process C4 and C5, the best inhibitors, are heterocyclic compounds containing several heteroatom's. These heteroatom's and aromatic rings named centres of adsorption interact easily with the metal surface [7, 12, 21, 24].

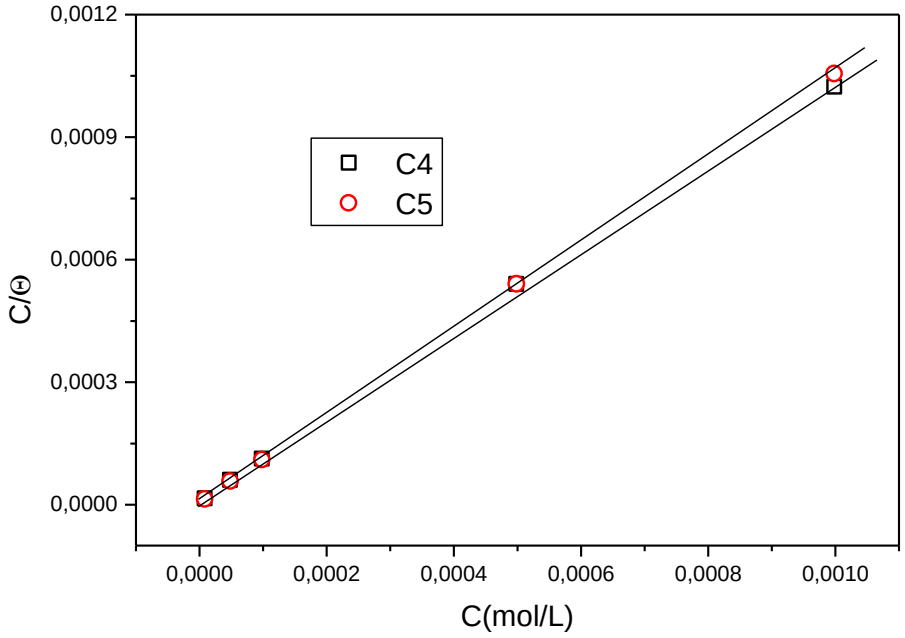

Figure 4. Langmuir isotherm of C4 and C5 on mild steel in 3.2M H_2SO_4 at 298 K.

Hence it can be suggested that each inhibitors adsorb on metallic surface forming strong chemisorptions bonds. This is in fact possible in view of the presence of unshared electron pairs in the organic compounds molecules and taking into consideration the behaviour of Fe as electrons acceptor as its d-sub monolayer is incomplete. The inhibitors studied may then be adsorbed via donor–acceptor interactions between the π-electrons of the aromatic systems and the unshared electrons pairs of the heteroatom's (-S, -N, -O) to form a bond with the vacant d orbital of the iron atom on the metal surface, which act as a Lewis acid, leading to the formation of a protective chemisorbed film.

Beside the fact that the inhibition phenomenon can be imputed to the presence of empty d-orbital in the Fe which led to an easier coordinate bond formation between the metal and inhibitors, these last contain nitrogen and oxygen atoms which are easily protonated in acid medium. Therefore, physical adsorption is also possible via electrostatic interaction between a negatively charged surface, which is provided with a specifically adsorbed anion on mild steel, and the positive charge of the inhibitors.

Table 9. Adsorption data of C4 and C5 on mild steel in 3.2M H_2SO_4

inhibitors	α	k_{ads}	$\Delta G°_{ads}$ (kJ mol^{-1})
C4	0,9992	112024,5	-38,78
C5	0,9999	257795,1	-40,85

3.7. Quantum chemical parameters

The B3LYP hybrid functional has shown to successfully predict a wide range of molecular properties. We rigorously assess the B3LYP functional for calculations of parameters, and thermo-chemical properties (atomization energies and reaction energies). The quantum calculations were performed using the Gaussian 03 program. The geometry of the studied compound was evaluated using the DFT level of the three-parameter compound functional of Becke (B3LYP) [22]. The 6-31G* basis set was used for all atoms. The geometry structure was optimized under no constraint. We have also examined HOMO and LUMO levels; the energy gap was evaluated as the difference between the HOMO and LUMO due to the MO energies [10, 42-44].

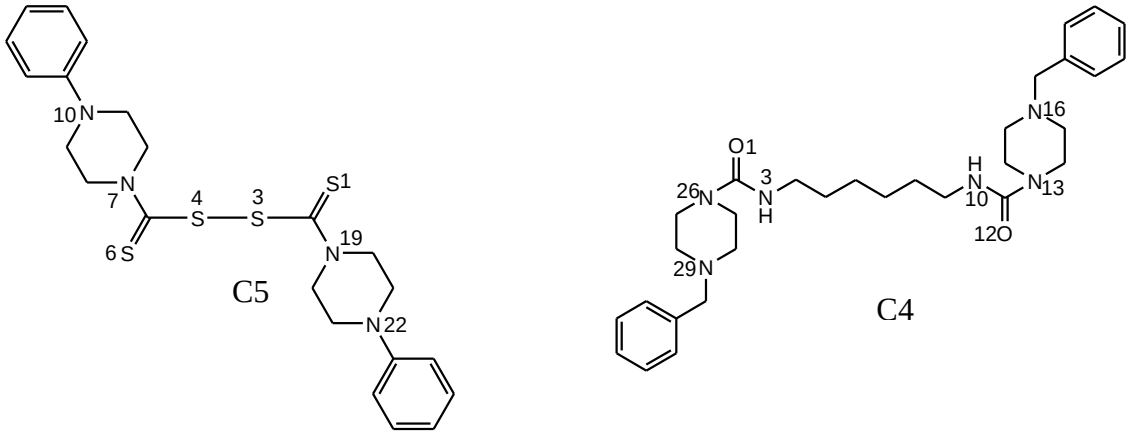

Schema 4. Molecular structure of C3 and C4

Table 9. Theoretical calculation of the total partial charge density of the heteroatom's of C4 and C4

	N (3), N (10)	N (13), N (26)	N (16), N (29)	O (1), O (12)
C4	-0,1189	-0,1044	-0,2972	-0,5269
	N (7), N (19)	N (10), N (22)	S (1), S (6)	S (3), S (4)
C5	-0,1352	-0,1884	-0,2001	-0,017

Mulliken charges arise from the Mulliken population analysis and provide a means of estimating partial atomic charges from calculations carried out by the methods of computational chemistry, particularly those based on the linear combination of atomic orbital's molecular orbital method, and are routinely used as variables in linear regression QSAR. The techniques described in the previous section were used to perform calculations of Mulliken atomic charges in C4 and C5 molecules (table9). These were compared with Mulliken charges calculated from DFT calculations using LCAO, basis sets with GAUSSIAN03. This during the atoms nitrogen, oxygen and sulfur having densities of negative charge total partial, are probably the active sites of adsorption of these compounds to the metal surface and this by forming coordination bonds with donor-acceptor orbital's vacant "d" of iron. Thus, it is important to note that the nitrogen atoms and negatively charged oxygen atoms are the anchor points of these compounds for the formation of complexes with iron. The theoretical calculation of the total partial charge density of hetero compounds C3 and C4, can reinforce the suggestion that the inhibitory effect contributed by the piperazine group is greater than that provided by the piperidine group

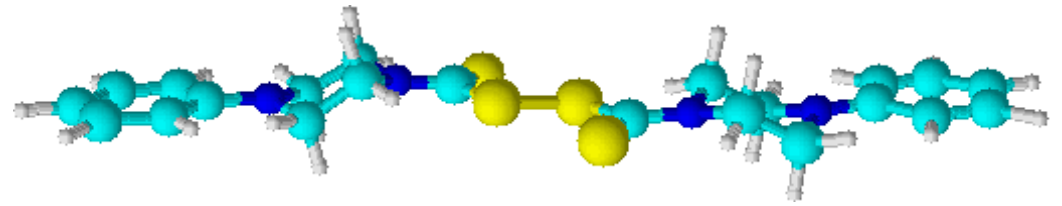

C5 (a)

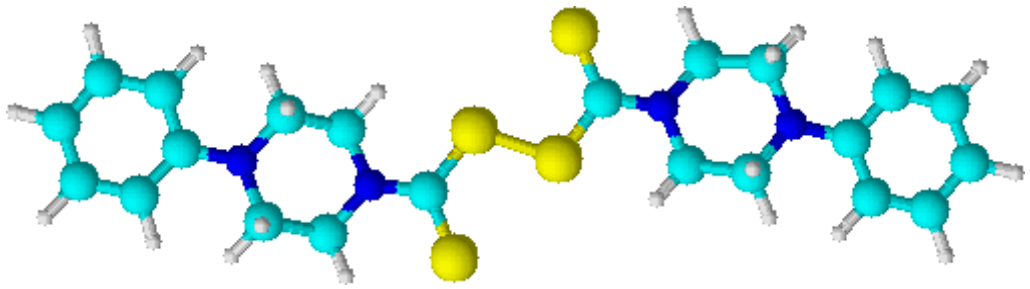

C5 (b)

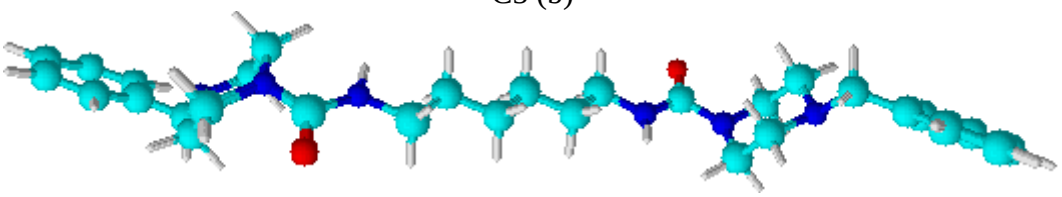

C4 (a)

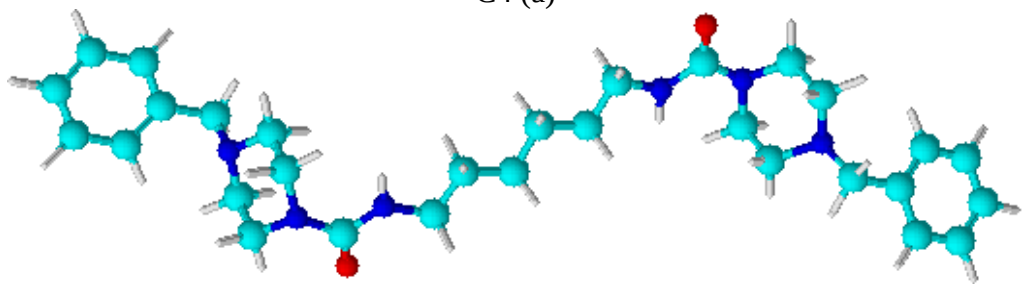

C4 (b)

Scheme 4. horizontal (a) and vertical (b) molecular structure for C3 and C4

The structure of compounds C4 is related to the C = O group, which creates more electron delocalization and therefore causes the stability of the structure. This results in an increase in electron density around nitrogen atoms, which gives an improvement in the coverage of the surface of the steel. The molecular structures optimized inhibitors C4 and C5 are given in schema 4.

Moreover, the presence of the disulfide in the organic structure makes the formation of a bond dπ-dπ resulting from overlapping of 3d electrons of the iron atom to empty 3d orbitals of the sulfur atom. The high efficiency of the inhibitor is attributed to the size of the molecule covering the surface and thereby inhibits corrosion of metal. In the compound C5 the presence of C2S4 group constituting the rigid centre of the molecule and its adsorption to the surface of the mild steel remains horizontal. There is, in this case, to a maximum of the reactive surface (Schema 4).

To confirm the results of quantum chemical calculations were performed for the compounds studied. to find a link between inhibition efficiency and molecular structure. An explanation based on quantum parameters of the inhibitors as highest occupied molecular orbital HOMO, lowest unoccupied molecular orbital LUMO and gap energies. Higher HOMO energy (E_{HOMO}) of the molecule means a higher electron donating ability and Low LUMO energy (E_{LUMO}) indicates that the acceptor accepts electrons easily. The quantum chemical indices and representation, ELUMO, EHOMO, dipole moment (μ) and the total energy of C2, C4 and C5 are reported in Table 10 and Schema 5. We note that the inhibition efficiencies of these molecules increase when ΔEgap decreases.

These results showed that the inhibition mechanism is based primarily on an adsorption process performed by charge transfer from the inhibitor to the metal. The increase in inhibition efficiency can be attributed to the difference ΔEgap. Over the energy band is low (in absolute value), plus the high inhibition efficiency

In the studied inhibitors, show that C2, C4 and C5 has both the highest HOMO and the lowest gap energies, this compounds transfers easily electrons are the best inhibitor. Moreover, the negative sign of the coefficient of E_{HOMO} can be concluded that the adsorption of these inhibitors on the steel surface has important. It is found a correlation between the inhibition efficiency with lower values of ΔE and μ dipole moment which was in a good agreement with the experimental findings. [31].

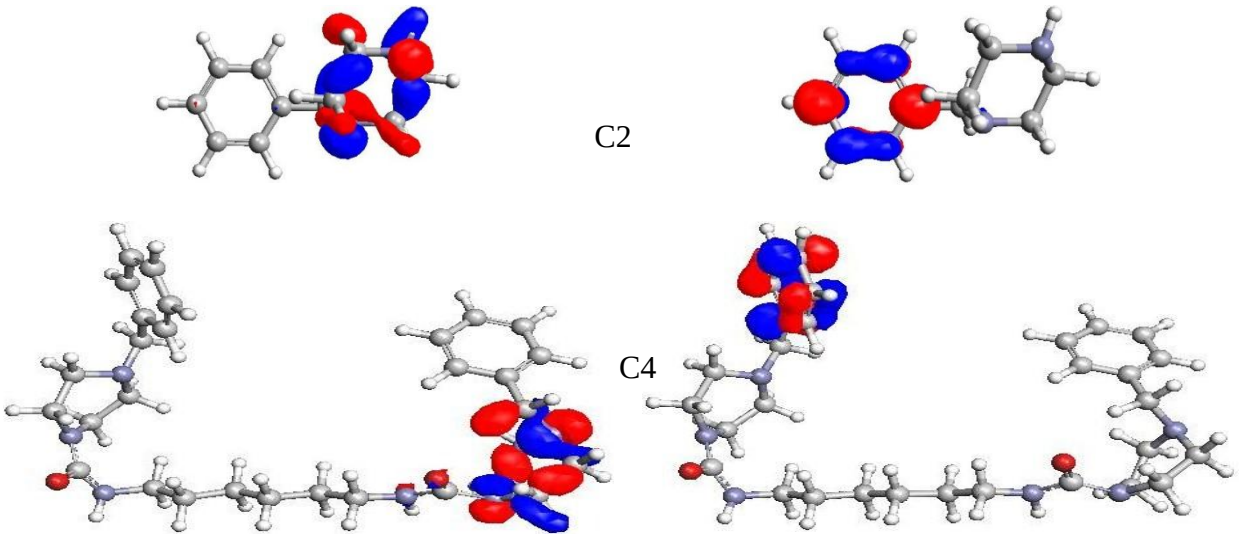

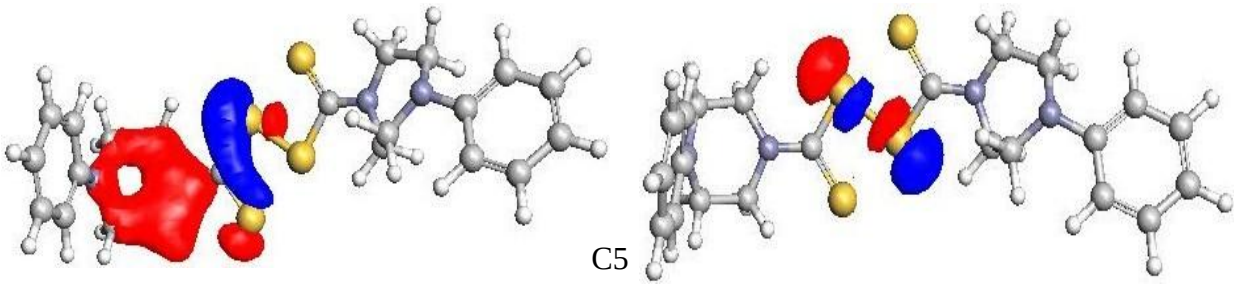

Scheme 5. Distribution density of HOMO and LUMO

The main difference between the molecular structures of these compounds is due to changes of the part (-CO-N-) and (-CS-S-) for C4 and C5. The main difference between these two molecules C4 and C5 is the density distribution of the HOMO is localized on thiocarbonyl in the case of the C5 molecule. This distribution thus ensures strong adsorption onto the metal surface (Schema 5).

Table 10. Quantum parameters of C1, C2, C3, C4, C5 and C6

Inhibitors	E_T (Kcal/mol)	μ (Debye)	E_{HOMO} (eV)	E_{LUMO} (eV)	ΔEgap (eV)
C2	$-333{,}6\ 10^3$	1,63	-8,80	3,84	12,64
C4	$-100{,}2\ 10^4$	1,64	-8,73	1,37	10,10
C5	$-165{,}7\ 10^4$	0,59	-7,07	1,39	8,46

The evaluation of inhibitory capacity revealed that the C5 is the most effective inhibitor in the conditions described above. Therefore, the main difference is the geometry of these molecules which can be explained by the number of oxygen atoms, sulfur and nitrogen. These atoms contribute to the chemisorptions of these molecules by way of links "donor-acceptor" between the nonbonding electrons of oxygen atoms, sulfur and nitrogen and π electron orbital's of the phenyl and "d" unsaturated metal. The molecule may be adsorbed also on the metal surface by horizontal (a) or vertical form (b), involving the displacement of water molecules from the metal surface.

4. CONCLUSION

It can be seen that the studied compound is good inhibitor for mild steel in 3.2 H_2SO_4 M

- The inhibition efficiency of C4 and C5 attains a maximum value around 95%, at 10^{-3} M.
- The addition of the C4 and C5 to a corrosive medium decreases the cathodic and anodic currents. It acts essentially as mixed-type inhibitor without modifying the mechanism of hydrogen evolution and this inhibition effect increases with the increase of inhibition concentration.

- Adsorption of the inhibitors fits a modified Langmuir isotherm model and physical adsorption type and adsorption model is suggested which is blocking it's active sites.
- The inhibition efficiency of the inhibitor C4 and C5 is closely related to the DFT quantum chemical parameters, (E_{HOMO}), energy of lowest unoccupied molecular orbital (E_{LUMO}), HOMO–LUMO energy gap, dipole moments and total energy (μ). The study of the HOMO and LUMO orbital's indicates that the preferred active sites for an electronic attack and the favourite sites for interaction with the metal surface are located within the region around the sulfur and nitrogen belonging to the piperazine compounds.
- The quantum theoretical calculations (Mulliken charges) are in good agreement with the result obtained from electrochemical study and structure - corrosion protection relationship which also confirm that the adsorption centre is S, N, O atoms.

L. Jiang, Y. Song, L. Tu, L. Sun, Y. Yu, H. Ge, G. Wei,

References

1. E&Mj-*Engineering and Mining Journal*, 213 (2012) 70.
2. V. Achal, A. Mukherjee, S. Goyal, M.S. Reddy, *Aci Materials Journal*, 109 (2012) 157.
3. N.V. Aieta, P.K. Das, A. Perdue, G. Bender, A.M. Herring, A.Z. Weber, M.J. Ulsh, *J. Power Sources*, 211 (2012) 4.
4. J.L. Alamilla, D. Campos, E. Sosa, *Structure and Infrastructure Engineering*, 8 (2012) 411.
5. P. Mohan, R. Usha, G.P. Kalaignan, V.S. Muralidharan, *Journal of Chemistry* (2013) ID 5411691.
6. L. Jiang, Y. Song, L. Tu, L. Sun, Y. Yu, H. Ge, G. Wei, *Materials Performance*, 51 (2012) 54.
7. A. Chetouani, K. Medjahed, S.S. Al-Deyab, B. Hammouti, I. Warad, A. Mansri, A. Aouniti, *Int. J. Electrochem. Sci*., 7 (2012) 6025.
8. J. Bell, C. Moore, L. Solis, G. Bell, *Materials Performance*, 51 (2012) 34.
9. R. Podor, N. David, C. Rapin, M. Vilasi, P. Berthod, *Corros. Sci*., 49 (2007) 3226.
10. M.J. Firdhouse, D. Nalini, *Journal of Chemistry* (2013).
11. M. Abdallah, I. Zaafarany, A.S. Fouda, D. Abd El-Kader, *J. Mater. Engin. Performance*, 21 (2012) 995.
12. I. Belfilali, A. Chetouani, B. Hammouti, A. Aouniti, S. Louhibi, S.S. Al-Deyab, *Int. J. Electrochem. Sci*., 7 (2012) 3997.
13. M. Kaddouri, M. Bouklah, S. Rekkab, R. Touzani, S.S. Al-Deyab, B. Hammouti, A. Aouniti, Z. Kabouche, *Int. J. Electrochem. Sci*., 7 (2012) 9004.
14. A.Y. Musa, A.A.H. Kadhum, M.S. Takriff, A.R. Daud, S.K. Kamarudin, N. Muhamad, *Corros. Engin. Sci. Technol*., 45 (2010) 163.
15. G. Mayakrishnan, S. Pitchai, K. Raman, A.R. Vincent, S. Nagarajan, *Ionics*, 17 (2011) 843.
16. Y. Abboud, B. Ihssane, B. Hammouti, A. Abourriche, S. Maoufoud, T. Saffaj, M. Berrada, M. Charrouf, A. Bennamara, H. Hannache, *Desalination and Water Treatment*, 20 (2010) 35.
17. Y.E. Kim, J.H. Choi, S.C. Nam, Y.I. Yoon, *J. Ind. Eng. Chem.*, 18 (2012) 105.
18. J.T. Zhang, Z.Q. Bai, J. Zhao, Y.R. Feng, Y. Wang, *Petroleum Sci. Technol*., 30 (2012) 1851.
19. A. Zarrouk, H. Zarrok, R. Salghi, B. Hammouti, F. Bentiss, R. Touir, M. Bouachrine. *J. Mater. Environ. Sci.* 4 (2) (2013) 177-192.
20. M. Bouklah, A. Attayibat, S. Kertit, A. Ramdani, B. Hammouti, *Appl. Surf. Sci.*, 242 (2005) 399.
21. S. El Ayyoubi, A. Chetouani, Hammouti, A. Warthan, A. Mansri, S.S. Al-Deyab, *Int. J. Electrochem. Sci*., 7 (2012) 1639.
22. A. Chetouani, K. Medjahed, K.E. Benabadji, B. Hammouti, S. Kertit, A. Mansri, *Prog. Org. Coat.*, 46 (2003) 312.

23. J.K. Sahu, K.K. Sahu, A.K. Ray, Proceedings of the Institution of Mechanical Engineers Part L-*Journal of Materials-Design and Applications*, 226 (2012) 34.
24. D. Bouzidi, A. Chetouani, B. Hammouti, S. Kertit, M. Taleb, S.S. Al-Deyab, *Int. J. Electrochem. Sci.*, 7 (2012) 2334.
25. A. Chetouani, M. Daoudi, B. Hammouti, T. Ben Hadda, M. Benkaddour, *Corros. Sci*., 48 (2006) 2987.
26. A. Chetouani, B. Hammouti, T. Benhadda, M. Daoudi, *Appl. Surf. Sci*., 249 (2005) 375.
27. A. Zarrouk, M. Messali, H. Zarrok, R. Salghi, A.A. Ali, B. Hammouti, S.S. Al-Deyab, F. Bentiss, *Int. J. Electrochem. Sci*., 7 (2012) 6998.
28. F. Bentiss, C. Jama, B. Mernari, H. El Attari, L. El Kadi, M. Lebrini, M. Traisnel, M. Lagrenee, *Corros. Sci.*, 51 (2009) 1628.
29. L. Herrag, B. Hammouti, S. Elkadiri, A. Aouniti, C. Jama, H. Vezin, F. Bentiss, *Corros. Sci*., 52 (2010) 3042.
30. M. Benabdellah, B. Hammouti, A. Warthan, S.S. Al-Deyab, C. Jama, M. Lagrenee, F. Bentiss, *Int. J. Electrochem. Sci.*, 7 (2012) 3489.
31. A. Chetouani, B. Hammouti, A. Aouniti, N. Benchat, T. Benhadda, *Progress in Organic Coatings*, 45 (2002) 373.
32. Y. Aouine, M. Sfaira, M.E. Touhami, A. Alami, B. Hammouti, M. Elbakri, A. El Hallaoui, R. Touir, *Int. J. Electrochem. Sci.*, 7 (2012) 5400.
33. R. Fuchs-Godec, M.G. Pavlovic, M.V. Tomic, *Industrial & Engineering Chemistry Research*, 51 (2012) 274.
34. Chris O. Akalezi, Conrad K. Enenebaku, Emeka E. Oguzie . *J. Mater. Environ. Sci*. 4 (2) (2013) 217-226
35. Y.Y. Andreev, *Protection of Metals and Physical Chemistry of Surfaces*, 48 (2012) 42.
36. J.D. Cao, K.J. Laws, N. Birbilis, M. Ferry, *Corros. Engin. Sci. Technol*., 47 (2012) 329.
37. K. Laarej, M. Bouachrine, S. Radi, S. Kertit, B. Hammouti, *E-Journal of Chemistry*, 7 (2010) 419.
38. K. Barouni, L. Bazzi, R. Salghi, M. Mihit, B. Hammouti, A. Albourine, S. El Issami, *Mater. Lett*., 62 (2008) 3325.
39. A. Chetouani, A. Aouniti, B. Hammouti, N. Benchat, T. Benhadda, S. Kertit, *Corros. Sci.*, 45 (2003) 1675.
40. S. Hassani, K.P. Roberts, S.A. Shirazi, J.R. Shadley, E.F. Rybicki, C. Joia, *Corrosion*, 68 (2012) 885.
41. L. Bammou, R. Salghi, A. Zarrouk, H. Zarrok, S.S. Al-Deyab, B. Hammouti, M. Zougagh, M. Errami, *Int. J. Electrochem. Sci*., 7 (2012) 8974.
42. M. Bouklah, H. Harek, R. Touzani, B. Hammouti, Y. Harek, *Arab. J. Chem.*, 5 (2012) 163.
43. N. Boussalah, S. Ghalem, S. El Kadiri, B. Hammouti, R. Touzani, *Res. Chem. Interm.*, 38 (2012) 2009.
44. S.K. Chen, S. Scheiner, T. Kar, U. Adhikari, *Int. J. Electrochem. Sci*., 7 (2012) 7128.